

Lab on a Chip

Accepted Manuscript



This is an *Accepted Manuscript*, which has been through the Royal Society of Chemistry peer review process and has been accepted for publication.

Accepted Manuscripts are published online shortly after acceptance, before technical editing, formatting and proof reading. Using this free service, authors can make their results available to the community, in citable form, before we publish the edited article. We will replace this *Accepted Manuscript* with the edited and formatted *Advance Article* as soon as it is available.

You can find more information about *Accepted Manuscripts* in the [Information for Authors](#).

Please note that technical editing may introduce minor changes to the text and/or graphics, which may alter content. The journal's standard [Terms & Conditions](#) and the [Ethical guidelines](#) still apply. In no event shall the Royal Society of Chemistry be held responsible for any errors or omissions in this *Accepted Manuscript* or any consequences arising from the use of any information it contains.

Cell culture on microfabricated one-dimensional polymeric structures for bio-actuator and bio-bot applications[†]

Sandeep V. Anand,^a M. Yakut Ali,^a and M. Taher A. Saif^{*a}

Here, we present the development, characterization and quantification of a novel 1D/2D like polymeric platform for cell culture. The platform consists of a 2D surface anchoring a long (few millimeters) narrow filament (1D) with a single cell scale (micro scale) cross section. We plate C2C12 cells on the platform and characterize their migration, proliferation, and differentiation patterns in contrast to 2D culture. We find that the cells land on the 2D surface, and then migrate to the filament only when the 2D surface has become nearly confluent. Individual and isolated cells randomly approaching the filament always retract away towards the 2D surface. Once on the filament, their differentiation to myotubes is expedited compared to that on 2D substrate. The myotubes generate periodic twitching forces that deform the filament producing more than 17 μm displacement at the tip. Such flagellar motion can be used to develop autonomous micro scale bio-bots.

1 Introduction

Bio-hybrid structures developed by combining mammalian cells with soft polymeric scaffolds have received much attention recently^{1,2}. Such structures, often termed as bio-actuators or bio-machines hold tremendous potential in various applications ranging from development of synthetic organs to drug screening, drug delivery, micro-surgery, sensing and actuation, autonomous or controlled directed motion (walking/swimming/crawling), transportation of cargo, information processing and other similar in-vivo and in vitro applications that require unconventional techniques and devices³⁻⁵.

In all of the aforementioned structures, the choice of the polymeric scaffold and the associated cell types determine their mechanical and bio-chemical properties and thus their functionalities. Polydimethylsiloxane (PDMS) is fast emerg-

ing as the polymer of choice for developing such bio-hybrid structures owing to its several unique properties - its excellent biocompatibility, transparency for a broad range of light spectra, robust mechanical properties, easy conjugation with ECM matrix proteins, negligible degradation in cell culture media at elevated temperatures for extended periods of time⁶⁻⁸.

Recent studies have successfully developed and demonstrated bio-actuators and bio-machines capable of performing some of the aforementioned tasks using clusters of mammalian cells in conjunction with soft polymeric scaffolds like PDMS and hydrogels. A 1-dimensional, microscale, bio-bot capable of swimming in fluids at low Reynolds number was developed using PDMS filaments³. Neonatal rat cardiomyocyte clusters cultured on PDMS filaments were used as actuators to achieve a propulsion speed of up to 10 $\mu\text{m}/\text{s}$ with a single filament. Propulsion speeds as high as 80 $\mu\text{m}/\text{s}$ were observed in swimmers with two filaments. Other stud-

^a Department of Mechanical Science and Engineering, University of Illinois at Urbana-Champaign, Urbana, Illinois 61801, USA. E-mail: saif@illinois.edu; Tel: 217-333-8552

[†] Electronic Supplementary Information (ESI) available

ies have utilized cardiomyocytes beating in clusters and conjugated with PEG hydrogels to achieve walking motion. Chan et al. developed a walking bio-bot powered by cardiomyocytes on 3D printed hydrogels⁴. Their design consisted of a 'biological bimorph' cantilever structure scaffold where cardiomyocytes act as actuators to drive the bio-bot. They were able to achieve walking speeds of up to 236 $\mu\text{m/s}$ in fluidic environments. Tanaka et al. developed micropumps by utilizing the contractions from a sheet of cardiomyocytes on PDMS scaffolds uniquely designed to pump fluids⁹. They were able to make fluid flow measurements using 1 μm polystyrene beads suspended in the fluid. The fluid oscillating frequency was observed to be 0.7 Hz and a linear displacement of upto 150 μm was observed. The fluid flow rate was measured to be 2 nL/min. They went on to further improve their design by wrapping a sheet of cardiomyocytes around spherical PDMS scaffold¹⁰. Swimming jellyfish like structures have been realized by culturing cardiomyocytes on thin elastomers arranged in freely moving lobes around a central disc¹¹.

There are several limitations to using primary cardiomyocytes for bio-bot applications, namely- cells are relatively large in size leading to space limitations on structures, scaling of force generated is not feasible as the cells do not multiply and proliferate, not very useful for co-culture with other cell types like neurons, primary cells are not feasible for long term experiments because they cannot be cryopreserved and require sacrificing of rats for each experiment. Skeletal muscle cells are viable alternatives to cardiomyocytes as functional components of futuristic bio-bot designs. This is due to some of the intrinsic advantages they present in terms of control and guidance, force scalability, robustness and most importantly

the ability to co-culture with other cell types. However, only a few studies have been reported that take advantage of skeletal muscle cells for bio-actuator and bio-bot applications. Skeletal muscles have been primarily utilized to study the active tension in Myotubes in isolation or in clusters on silicon, PDMS and collagen¹²⁻¹⁴. Other applications include the development of engineered skeletal muscle tissues in 3D. Engineered skeletal muscle was developed using myotubes and synthetic tendons¹⁵⁻¹⁷. Other methods to develop skeletal muscle tissues include culturing myotubes in pre-fabricated scaffolds and suspending between PDMS pillars¹⁸.

In this study we report the development of a novel 1D polymeric platform and culture technique to form C2C12 derived myotube filaments. Patterns of cell migration and mitosis on the 1D substrate are reported. Parameters like nuclei orientation, spread area, deformation and cell density on the 1D substrate are quantified and compared with those on flat PDMS substrates. Techniques for precise control of cell placement on the 1D structure are outlined. Finally, methods for myotube formation and eventual bio-actuator realization are described. The novel techniques presented here will be useful in improving the performance and functionalities of existing micro-swimmers and future biological machines by integrating subunits like neurons and vascular networks for control and guidance of biobots and for other higher order functions.

2 Materials and methods

2.1 Silicon mold and device fabrication

The 1D PDMS structures were fabricated using a previously developed process¹⁹ by the authors. Briefly, a silicon wafer was patterned and etched using standard microfabrication

techniques as shown in Fig. 1(a-b). Photoresist was spun coated on a 4" Si wafer and patterned using standard photolithography techniques. The wafer was then etched using a dry etching process in an inductively coupled plasma reactive ion etching (ICP-DRIE) machine. The etch depth and thus the depth of the final PDMS structure was determined by the etch time. A thin layer of polytetrafluoroethylene (PTFE) was deposited on the wafer after the completion of the etching process to lower the adhesion of PDMS to the Si wafer and to prevent delamination of the structures during peeling off from the molds. The device design was such that there were 4-5 microchannels of width 7-10 μm and 2-3 mm in length connected by squares of 3 mm edges on either sides. These squares are referred to as reservoirs where PDMS (Sylgard 184, 4:1 base to crosslinker ratio) was poured as shown in Fig. 1(c). Liquid PDMS filled the microchannels in about 2 minutes due to capillary draw¹⁹ as shown in Fig. 1(d). PDMS in the molds was then cured at 60° C for 12 hours. The molds with the cured PDMS structures were submerged in ethanol for about 15 mins to allow PDMS to swell, which facilitated the peeling process. The structures were then released manually and transferred to polystyrene petri dishes and thoroughly rinsed in PBS before extracellular matrix functionalization. A schematic diagram of the finally peeled PDMS structure is shown in Fig. 1(e). The scanning electron micrographs of the final structures are shown in Figs. 1(f-g).

2.2 1D substrate preparation and extracellular matrix functionalization

The structures were air dried after rinsing at room temperature for 2-3 hours in a sterile environment. Fibronectin (BD

Bioscience, 25 $\mu\text{g}/\text{mL}$) was the preferred extracellular matrix for cell attachment on the structures. They were incubated in fibronectin for about 3 hours after which they were again rinsed in PBS 2-3 times. Following ECM functionalization, the structures were transferred onto two different types of substrates depending on the experiments to be performed. For the purpose of high resolution immunofluorescence imaging the structures were transferred onto a glass bottom petri-dish. For the purposes of time lapse imaging and bio-actuator experiments they were transferred to another substrate which was custom prepared to minimize cell adhesion. These substrates were prepared by gluing two square silicon chips of 4mmX4mm edge and 500 μm thickness separated by a distance equal to the length of the 1D structure (filaments) and incubating the entire substrate in Pluronic F127 (1% in PBS, Sigma-Aldrich) for 20 mins to ensure negligible cell adhesion on regions without ECM. The ECM coated PDMS structures were then mounted on the Si chips. The Si chips acted as suspenders which prevented any kind of interaction between the cells on the filaments and those on the petri-dish. The final configuration of the PDMS structure mounted on Si chips in a petri-dish is shown in Fig. 2(a). Cells of required density were plated on the structures as shown in Fig. 2(b). The cells landing on the PDMS surface adhered, while the others remained rounded and were washed away during subsequent media change procedures. The attached cells elongated and eventually started to proliferate and move towards the 1D filaments as shown in Fig. 2(c).

2.3 Cell culture and imaging

C2C12 myoblast cells (ATCC, Manassas, VA) were cultured in growth media (GM) composed of DMEM (Life Technologies, Grand Island, NY, Cat. No. 41965-039) supplemented with 10% fetal bovine serum (ATCC, Manassas, VA, Cat. No. 30-2020) and 1% Penicillin-Streptomycin (ATCC, Manassas, VA, Cat. No. 30-2300). The C2C12 myotubes in GM were seeded on the ECM functionalized structures at a cell density of about 200,000 cells/cm² and incubated at 37⁰ C and 5% CO₂ for 1 hour before any experiments were performed. The process of differentiation to myotube was initiated by replacing GM with fusion media (FM) comprising of 2% horse serum (ATCC, Manassas, VA, Cat. No. 30-2040) in place of the fetal bovine serum in GM. One hour after plating the cells on the suspended structures, time lapse imaging in phase contrast mode was carried out using an Olympus IX81 microscope with an incubation chamber. The filaments were observed at 10X magnification in an environmental chamber under biological conditions. Images were captured automatically at 2 minute intervals for 40 hours.

2.4 Immunohistochemistry and fluorescence imaging

The cells were first washed three times with PBS and then fixed with 4% paraformaldehyde in PBS for 15 min at room temperature. Next, they were permeabilized with 0.3% Triton-X100 for 3 min and blocked in 5% Bovine Serum Albumin (BSA) for 10 min at room temperature. The cells were then immunostained with monoclonal sarcomeric myosin antibody MF-20 (Developmental Studies Hybridoma Bank, Iowa City, IA) for 1h at room temperature and rinsed 3 times with PBS. F-actin staining was done using tetramethylrhodamine

(TRITC) conjugated phalloidin (Sigma-Aldrich, MO) at 50 µg/mL concentration for 1h at room temperature followed by a PBS rinse. Finally, nuclei were stained using DAPI (1:1000) for 20 min at room temperature. The samples were incubated in PBS overnight and imaged using a Zeiss LSM 700 confocal scanning laser microscope.

3 Results and discussion

3.1 Unique cellular migration and mitosis

Time lapse imaging of the C2C12 myoblasts for extended periods of time revealed their migration patterns and cellular mitosis on 1D substrates. Figs. 3(a-j) show a set of phase contrast images obtained over 40h after the cells were plated. The entire time lapse may be viewed in supplementary video S1. Note that the geometry of the 1D substrate contains irregularities in the form of notches and groves. The plated cells preferentially landed on the reservoir pads with large flat surface area instead of the filaments. Almost no cell landed on the filament due to its narrow width (<10 µm). Fig. 3(a) shows the filament along with the grove 1h after cell plating when time lapse imaging started. Over time the cells started to migrate towards the filaments from both the reservoirs. Part of a cell was first spotted 8h 20 min after the beginning of the time lapse as represented by the arrow in Fig. 3(b). The single cell, without the influence of any other cells in its vicinity, moved towards the groves from right to left of the image (Fig. 3(c)). The cell constantly sensed its microenvironment by extending its filopodia. The moment the cell sensed the presence of the groves (Fig. 3(d)) it returned towards the reservoir following the same path that it had taken to reach the grove (Fig. 3(e)), and completely disappeared from the field of view (Fig. 3(f))

as it moved further towards the right of the image towards the reservoir. As time progressed, cells began to divide and proliferate in and around the reservoirs and the free space available for the cells to migrate and expand starts to shrink. As a result, the cells were forced to move towards the grove due to 'peer pressure' (Fig. 3(g)). More and more cells started to appear in the field of view as they were forced to make their way towards the filaments from either side, bridging the groves (Fig. 3(h)). After about 29h the cells were completely confluent on the filament. During mitosis the cells partially detached themselves from the 1D substrate, assumed a spherical morphology and appeared to be dangling from the structure as shown in Fig. 3(h,i). The daughter cells merged with the rest of the cells and adhered to the 1D substrate. In the course of the time lapse many cells divided in the same way and migrated and merged with other cells. At the end of the time lapse around the 40h time mark (Fig. 3(j)), several cells could be observed in spherical morphologies and the entire structure was confluent with at least one layer of cells. The velocities of the cells under different circumstances are quantified in the next section.

3.2 Migration velocities

Migration velocities of the cells at various different stages of the time lapse observation were calculated using a simple particle tracking cross-correlation algorithm in MATLAB. Fig. 4(a) shows the displacement of the first observable cell (Fig. 3(b-e)) as a function of time. The migration velocity of the cell on the smooth part of the 1D surface under no influence from other cells seemed to be fairly constant (at about $1 \mu\text{m}/\text{min}$). The cell suddenly stopped when it encountered the groves indicated by the flat region in the curve. Interestingly, the cell

did not stay at rest for too long- instead it reversed its direction and moved at a much faster rate (almost twice the forwards velocity) to return towards the reservoir. Fig. 4(b) represents the instantaneous forward and return velocities of single cells under various circumstances. The 'single' case indicates cell moving in isolation without the influence of other cells. The forward and return velocities in this case were $1.05 \mu\text{m}/\text{min}$ and $1.94 \mu\text{m}/\text{min}$ respectively. Multiple 'case' indicates a single cell under the influence of multiple cells. The velocities in this case were $2.26 \mu\text{m}/\text{min}$ and $4.79 \mu\text{m}/\text{min}$. Finally 'new' indicates the velocities of newly formed cells immediately after cell division migrating with a forward and return velocity of $1.71 \mu\text{m}/\text{min}$ and $3.6 \mu\text{m}/\text{min}$ respectively. In all the cases it was observed that the return velocity was almost twice the forward velocity indicating biophysical bias towards quick change in directions. It may also be noted that the cells under the influence of other cells tended to move faster in either directions when compared to isolated cells. This indicates that the cell migration on 1D substrates is dependent on and affected by the phenomena of 'crowding' and 'peer pressure'. Actin and nuclei distribution of the cells are characterized and quantified in the next few sections.

3.3 Actin and nuclei distribution

The actin and nuclei distribution of the C2C12 myoblasts on the 1D filaments and plain PDMS are as shown in Figs. 5(a-i). These images were obtained after fixing and staining the myoblasts for 24h after plating them on the structures. The cells were still in the growth medium (GM) and hadn't started to fuse into myotubes. Figs. 5(a-c) show the actin and nuclei distributions of the cells at a relatively lower magnification

of 10X in order to visualize the intersection between the filaments and the reservoir (left of the images). Dense clustering of actin was observed at the intersection. The cells seemed to be uniformly distributed forming a confluent layer over the filament. The nuclei seemed to be fairly well aligned along the length of the filament (Figs. 5(d-f)). The actin distribution seemed to be fairly uniform and dense over the entire structure. Furthermore, the nuclei seemed to be elongated and stretched assuming an ellipsoid morphology. We believe this happens due to the geometric confinement of the cells on the surface of the filaments. Similar morphologies of cells were observed in the literature when plated on patterned 1D shapes like lines on soft substrates like PA gels^{20,21}. Figs. 5(g-i) show the actin and nuclei distribution of the cells plated on flat, large area, PDMS substrates. It may be noticed that the nuclei orientation and actin distribution have no specific pattern of organization. Instead, they seem to be more random when compared to the filament case as there is no geometric confinement of the cells.

3.4 Three dimensional characterization

Three dimensional fluorescence images were recreated from the confocal z-stacks of the cells on the filaments (see supplementary movies S2-S4). The Z resolution of the stacks was about 0.7 μm . Cells completely wrapped around the filaments from all four sides as opposed to just attaching on the sides with the highest surface areas (Figs. 6(a-c)). One would have expected the cells to migrate from the thinner sides to the wider sides in order to spread out. But it appears that the cells occupied all the surfaces evenly. However, it must be noted that the morphologies of the nuclei and actin distribu-

tion are different on the top surface and the edges than on the sides. The nuclei on the sides and edges seemed to be more deformed as compared to those on the wider top surface. The actin density was higher along the edges. The nuclei seemed to be flattened due to the actin network passing over them and exerting downward forces. It also appeared that the cells had accumulated at the bottom of the filaments too although at a lower density as compared to the top side.

3.5 Nuclei orientation

The orientation angle of the nuclei (about 40 cells) of C2C12 myoblasts on the filaments and flat PDMS is measured using ImageJ. The data is represented in a polar plot (Fig. 7(a-b)). On the filament structure most of the nuclei were oriented between $160 - 180^\circ$ (around 22 cells) indicating that the cells aligned themselves along the length of the filaments. This is due to the geometric confinement of the cells on the filaments as discussed in the previous section. The nuclei on flat PDMS substrates did not show orientation bias towards any direction as can be noted from Fig. 7(b). The orientation angles were spread over $0 - 180^\circ$. This indicates that given the freedom to grow, proliferate, migrate and expand on flat PDMS substrates without any microscopic geometric constraints, the cells will orient themselves randomly.

3.6 Nuclei deformation and spreading

Nuclei spread area of the C2C12 myoblasts on the filaments and flat PDMS was calculated using ImageJ. Box plots of nuclei spread area shown in Fig. 7(d). The circular markers at the center of the shaded boxes represent the mean nuclei spread area. The horizontal lines through the shaded boxes

indicate the median nuclei spread area and the lower and upper edges represent the 25th and 75th percentile, respectively. The whiskers extending vertically from each box represent the standard deviation. The median nuclei spread area of the cells on the filament was about 90 μm^2 whereas in the case of flat PDMS substrate the nuclei spread area was much higher at 130 μm^2 . This indicates that the narrow geometry of the structures tend to compact the cells thus leading to a smaller median spread area. On the other hand the cells can spread freely on flat PDMS substrates as there are no geometric constraints. A direct consequence of the compaction effect produced by the filaments was the increased cell density as shown in the histograms in Fig. 7(c). There were more than 40 cells per 10000 μm^2 area of the structure as compared to about 35 cells per 10000 μm^2 on flat PDMS substrates. The higher density of nuclei is expected to produce thick myotubes in relatively shorter time frame compared to PDMS substrates. The lateral deformation of the nuclei is quantified using a parameter called the circularity index of the nuclei using ImageJ. Circularity index (CI) was calculated using the relation, $CI = 4 \times \pi \times [\text{Area}]/[\text{perimeter}]^2$. Hence, a $CI = 0$ indicates an infinitely elongated polygon and a $CI = 1$ indicates a perfect circle. CI of nuclei on the filament was estimated to be about 0.6 while that of the nuclei on flat PDMS is estimated to be about 0.8 as shown in Fig. 7(e).

3.7 Myotube formation

The C2C12 myoblasts were incubated in fusion media (FM) after 24h of cell plating. Fully differentiated myotubes were obtained on the filaments after 6 days in the FM (Fig. 8). Myotubes extended all the way from the reservoir to the fila-

ments as shown in the phase contrast image in Fig. 8(a). Furthermore, we were able to control the placement and length of myotubes on the PDMS structure through spatial patterning of ECM and pluronic F127 (Fig. 8(b)). One side of the structure was made to adhere to the petri-dish surface through stiction, and ECM was carefully placed over the reservoir and 300-400 μm of the exposed PDMS structure. Once, the ECM was conjugated to the exposed surface, the entire structure was released and incubated in pluronic F127 leading to a very specific region of interest where myotubes could grow (see Fig. 8(b)). The nuclei, actin and myosin organization of the differentiated myotubes are as shown in Fig. 8(c-f). The myosin organization in these images was of particular interest as it showed the formation of thick myotubes around the filament in a very short span of 6 days. It usually takes longer to fuse myotubes on PDMS substrates (between 10-14 days)²². The reason for the myotube fusion in such short duration may be due to the alignment and compaction of the C2C12 myoblasts achieved through geometric confinement on the filaments. It is reported in the literature that myoblasts cultured on line patterns on 2D substrates fuse faster than those cultured on flat substrates^{22,23}. Such functionality is highly desirable in bio-actuators and micro-swimmers.

3.8 Bio-actuator characterization

Fully differentiated myotubes are known to twitch and contract^{24,25}. We made use of this property of the myotubes to develop periodically contracting bio-actuators. We cultured the myoblasts on suspended filaments and differentiated the cells to form myotubes. Once the myotubes were formed after about six days of culture in fusion media, one end of the

filament was manually cut off such that it resembled a cantilever beam. Fig. 9 shows such a structure with Myotubes cultured all along the length of the filament. The filament doesn't look straight anymore because the regions with higher density of Myotubes are deformed due to the higher traction stresses applied by the Myotubes. A contracting myotube was observed close to the base of the cantilever as shown in Fig. 9. This Myotube produced enough periodic contractile force to actuate the entire beam (see supplementary movie S5). We tracked the displacements of three distinct points separated by few hundred micro meters along the length of the beam using simple particle tracking cross-correlation algorithm in MATLAB. The view graphs on the right show the horizontal and vertical displacement profiles of the three points labeled in the phase contrast image. As can be seen, the peaks of the three curves on both the plots align perfectly (although with varying magnitudes) indicating that there is just one source of actuation on the beam. The maximum peak displacement was observed to be as high as 17 μm for point 3. Such deformations may be utilized to develop autonomous biobots. Note that here the bio-actuator contracts purely based on spontaneous twitching of the myotubes. The contraction of the bio-actuator due to spontaneous twitching of myotubes implies that swimming bio-bots similar to those demonstrated before³ but with much higher control and improved functionalities may be obtained using the described methods. Furthermore, it may be possible to enhance the contraction magnitude and frequencies using electrical and optogenetic means. Work is already underway to develop electrically and optogenetically actuated micro-swimmers using C2C12 derived myotubes by the authors and shall be reported in future publications.

4 Conclusions

A novel 1D polymeric platform and a cell culture methodology have been developed, characterized and quantified for robust bio-actuator and bio-bot development using C2C12 cells. The developed techniques are expected to improve the performance and functionalities of existing micro-swimmers and future biological machines by allowing the capability to integrate subunits like neurons and vascular networks for control and guidance and other higher order functions. The unique geometry of the 1D filaments enhances cell density and increases cellular compaction, thus leading to the formation of mature and thick myotubes in shorter time frames with autonomous contraction capability. Cellular migration and mitosis pattern on the 1D substrate has been characterized by observing migrating cells on the filaments under various geometric conditions. Precise control of Myotube placement on the filaments has been demonstrated through spatial patterning of ECM proteins and cell repellent molecules. An example bio-actuator design capable of autonomous contraction has been demonstrated. The developed platforms and techniques will be used to realize electrically and optogenetically controlled bio-bots in the near future.

5 Acknowledgements

This project was funded by the National Science Foundation (NSF), Science and Technology Center on Emergent Behaviors in Integrated Cellular Systems (EBICS) Grant CBET-0939511. Immunostaining and confocal microscopy imaging were performed at the Institute for Genomic Biology (IGB), UIUC.

References

- 1 V. Chan, H. H. Asada and R. Bashir, *Lab on a chip*, 2014, **14**, 653–70.
- 2 R. D. Kamm and R. Bashir, *Annals of biomedical engineering*, 2014, **42**, 445–59.
- 3 B. J. Williams, S. V. Anand, J. Rajagopalan and M. T. A. Saif, *Nature communications*, 2014, **5**, 3081.
- 4 V. Chan, K. Park, M. B. Collens, H. Kong, T. A. Saif and R. Bashir, *Scientific reports*, 2012, **2**, 857.
- 5 C. Cvetkovic, R. Raman, V. Chan, B. J. Williams, M. Tolish, P. Bajaj, M. S. Sakar, H. H. Asada, M. T. A. Saif and R. Bashir, *Proceedings of the National Academy of Sciences of the United States of America*, 2014, **111**, 10125–10130.
- 6 D.-H. Kim, P. K. Wong, J. Park, A. Levchenko and Y. Sun, *Annual review of biomedical engineering*, 2009, **11**, 203–33.
- 7 J. Park, J. Ryu, S. K. Choi, E. Seo, J. M. Cha, S. Ryu, J. Kim, B. Kim and S. H. Lee, *Analytical chemistry*, 2005, **77**, 6571–80.
- 8 Y. Zhao, C. C. Lim, D. B. Sawyer, R. Liao and X. Zhang, *Cell motility and the cytoskeleton*, 2007, **64**, 718–25.
- 9 Y. Tanaka, K. Morishima, T. Shimizu, A. Kikuchi, M. Yamato, T. Okano and T. Kitamori, *Lab on a chip*, 2006, **6**, 362–8.
- 10 Y. Tanaka, K. Sato, T. Shimizu, M. Yamato, T. Okano and T. Kitamori, *Lab on a chip*, 2007, **7**, 207–12.
- 11 J. C. Nawroth, H. Lee, A. W. Feinberg, C. M. Ripplinger, M. L. McCain, A. Grosberg, J. O. Dabiri and K. K. Parker, *Nature biotechnology*, 2012, **30**, 792–7.
- 12 H. Fujita, T. Van Dau, K. Shimizu, R. Hatsuda, S. Sugiyama and E. Nagamori, *Biomedical microdevices*, 2011, **13**, 123–9.
- 13 H. Fujita, K. Shimizu and E. Nagamori, *Biotechnology and bioengineering*, 2010, **106**, 482–9.
- 14 Y. Sun, R. Duffy, A. Lee and A. W. Feinberg, *Acta biomaterialia*, 2013, **9**, 7885–94.
- 15 R. C. Strohman, E. Bayne, D. Spector, T. Obinata, J. Micou-Eastwood and A. Maniotis, *In vitro cellular & developmental biology : journal of the Tissue Culture Association*, 1990, **26**, 201–8.
- 16 R. G. Dennis and P. E. Kosnik, *In vitro cellular & developmental biology. Animal*, 2000, **36**, 327–35.
- 17 R. G. Dennis, P. E. Kosnik, M. E. Gilbert and J. A. Faulkner, *American journal of physiology. Cell physiology*, 2001, **280**, C288–95.
- 18 H. Vandenberg, S. Swadison and P. Karlisch, *FASEB J*, 1991, **5**, 2860–2867.
- 19 J. Rajagopalan and M. T. A. Saif, *Journal of Microelectromechanical Systems*, 2013, **22**, 992–994.
- 20 A. Engler, L. Bacakova, C. Newman, A. Hategan, M. Griffin and D. Discher, *Biophysical Journal*, 2004, **86**, 617–628.
- 21 M. Théry, *Journal of cell science*, 2010, **123**, 4201–13.
- 22 W. W. Ahmed, T. Wolfram, A. M. Goldyn, K. Bruellhoff, B. A. Rioja, M. Möller, J. P. Spatz, T. A. Saif, J. Groll and R. Kemkemer, *Biomaterials*, 2010, **31**, 250–8.
- 23 P. Bajaj, B. Reddy, L. Millet, C. Wei, P. Zorlutuna, G. Bao and R. Bashir, *Integrative biology : quantitative biosciences from nano to macro*, 2011, **3**, 897–909.
- 24 K. Nagamine, T. Kawashima, T. Ishibashi, H. Kaji, M. Kanzaki and M. Nishizawa, *Biotechnology and bioengineering*, 2010, **105**, 1161–7.
- 25 S. T. Cooper, A. L. Maxwell, E. Kizana, M. Ghodussi, E. C. Hardeman, I. E. Alexander, D. G. Allen and K. N. North, *Cell motility and the cytoskeleton*, 2004, **58**, 200–11.

Figure captions

Figure 1: One dimensional PDMS structure fabrication methodology. Si micro-molds are prepared using photolithography and dry etching of Si wafers. (a) Photoresist is patterned on a Si wafer using standard photolithography techniques. The wafer is then etched in an inductively coupled plasma- deep reactive ion etching (ICP-DRIE) machine to the desired depth. (b) The etched wafer is then coated with polytetrafluoroethylene (PTFE) covering the side walls and the bottom surfaces of the micro channels. PDMS (4:1 base to cross-linker ratio) droplets are poured on the reservoirs of the micro-channels. (c) The PDMS fills the micro-channels through capillary draw. (d) Solid 1D PDMS structures connected by the reservoirs may be peeled off after curing at 60° C for 12 hours. (e) Scanning electron micrograph of the cured 1D PDMS structures showing a smooth and continuous topography (f) Zoomed SEM image showing a single device with a broad region closer to the reservoir transitioning smoothly to a thinner structure.

Figure 2: Final PDMS structure configuration and cell plating. (a) Shows the final configuration of the PDMS structure on the Si chips in a petri dish just before cell plating. The PDMS structure is coated with ECM while all the other surfaces are coated with pluronic F127. (b) Schematic of rounded cells on all the 2D surfaces immediately after cell plating. Note that the cells do not land on the 1D regions due to limited surface area available to adhere. (c) Elongated cells after several hours of plating. Cells divide and proliferate after few hours of plating. Once, the reservoirs are confluent, the cells start moving towards the 1D structure and eventually cover the whole structure.

Figure 3: Time lapse imaging of C2C12 myoblasts over 40 hour. (a) Free standing device coated with fibronectin after one hour of cell plating. (b) A single cell starts to appear on the right side of the image as indicated by the arrow. (c) The cell is now entirely in view and it is moving towards the groves along the side of the filament. (d) The filopodia of the cell extend and sense the presence of the groove as an irregularity in the topology. (e) The cell doesn't proceed forward anymore and returns. (f) The cell completely exits the field of view moving further towards the reservoir from where it came. (g) A cell reappears along with several other cells moving in a group as the free space in and near the reservoir region is starting to shrink as a result of proliferating and migrating cells crowding the area. (h) The cells temporarily detach from the device to form spherical structures just before cell division. (i) The newly formed cells from the dividing spheres are shown by the arrows. (j) At the end of the time lapse the entire structure is confluent with cells. Several spherical structures may be observed indicating that many cells are at the stage of division at this point. (k-l) Zoomed in images of the highlighted regions in (i) and (j) respectively showing a confluent layer of cells and newly formed cells on the structure. (Scale bar: 100 μm)

Figure 4: Displacement tracking and velocity data from the time lapse images. (a) Shows the horizontal tracking data of a

single point on a cell moving in isolation without the influence of any other cells during the initial phase of the timelapse. (b) Instantaneous forward and return velocities of single cells under various different circumstances.

Figure 5: Actin and nuclei organization of C2C12 myoblasts on the 1D PDMS devices and plain PDMS substrates. (a-c) show the actin and nuclei organization of the cells on the PDMS devices at 20X magnification (Scale bar: 100 μm). (d-f) show the actin and nuclei organization of the cells on the PDMS devices at 40X magnification. The nuclei seem to be elongated and the actin fibers show a directional preference along the length of the device. (g-i) show the actin and nuclei organization of the cells on plain PDMS. (Scale bar: 25 μm).

Figure 6: Three dimensional visualization of the PDMS device confluent with C2C12 myoblast cells on all sides. (a-c) show the three dimensional nuclei and actin organization of the C2C12 cells on the top and side surfaces of the PDMS structure. It may be observed that the nuclei on the edges and sides are more deformed than the ones on the top surface. (d-f) show the cross sectional view of the nuclei and actin distribution on the PDMS device. It may be observed that the cells wrap around the device completely but in a non-uniform manner. The device dimensions in the image are 200X30X10 μm . (Scale bar: 50 μm)

Figure 7: Quantitative comparisons of the nuclei orientation, deformation and cell spreading on the 1D devices and flat PDMS substrates. (a-b) show polar plots representing the nuclei orientation angles of the C2C12 cells on 1D PDMS structures and flat PDMS substrates respectively. Angles closer to 0° and 180° imply nuclear orientations along the neutral axis of the 1D PDMS beam. It may be observed that the nuclei on the 1D device tend to be oriented along the beam axis while those on the flat PDMS substrates have no particular orientation bias. (c) shows a bar plot of the cell density on 1D device and flat PDMS substrate. The cell density is calculated by counting the number of nuclei within a given area. (d-e) show box plots of nuclei spread area on 1D device and flat PDMS substrate. The circular marker in the center of the shaded box represents the mean nuclei spread area. The horizontal line through the shaded box indicates the median nuclei spread area and the lower and upper edges represent the 25th and 75th percentile, respectively. The whiskers extending vertically from each box represent the standard deviation. (f-g) show box plots of nuclei circularity index on 1D structure and flat PDMS substrate. Circularity is calculated using the relation: $\text{circularity} = 4 \times \pi \times [\text{Area}] / [\text{perimeter}]^2$. Hence, 0 indicates an infinitely elongated polygon and 1 indicates a perfect circle.

Figure 8: Characterization of fully differentiated C2C12 derived myotubes on the 1D PDMS substrates. (a) shows a phase contrast image of fully matured myotubes after day 6 of cell plating. (b) shows a phase contrast image of Myotube formation on only one side of the PDMS device through selective patterning of fibronectin (scale bar: 50 μm). (c-f) show nuclei, actin and myosin organization in the differentiated myotubes after day 6 of cell plating. The myotube formation observed through myosin

staining indicates total maturation around the 1D device and extending along the length of the device.

Figure 9: Demonstration of Myotube powered bio-actuator. The phase contrast image shows fully differentiated myotubes formed along the length of the 1D structure which is released at one end to behave like a soft cantilever beam. The spontaneous periodic twitching of the myotubes closer to the base of the cantilever (indicated by the dashed circle) deforms the entire beam in a cyclic fashion. Other dense myotubes (denoted by arrows) exert enough traction forces to bend and deform the beam. The view graphs on the right show the horizontal and vertical displacements of three different points (denoted as points 1-3) on the beam as the myotube close to the base contracts periodically. (Scale bar: 100 μm)

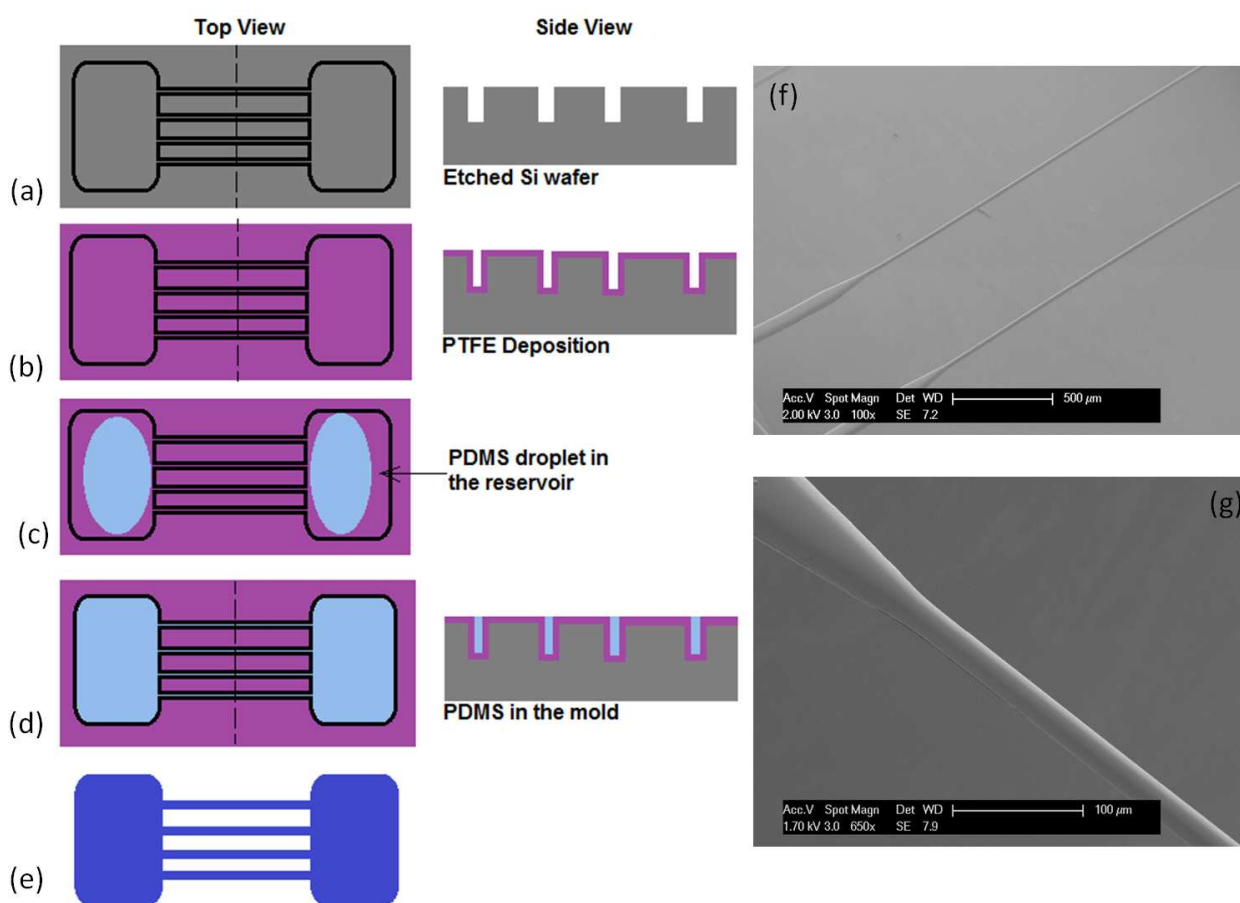


Fig. 1

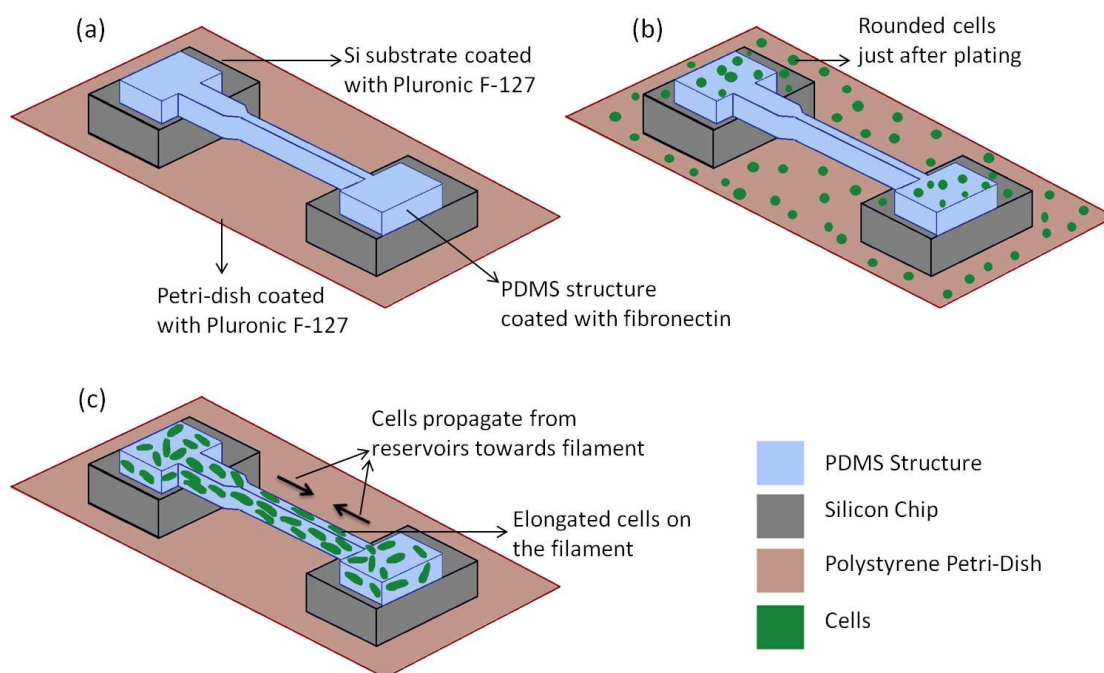


Fig. 2

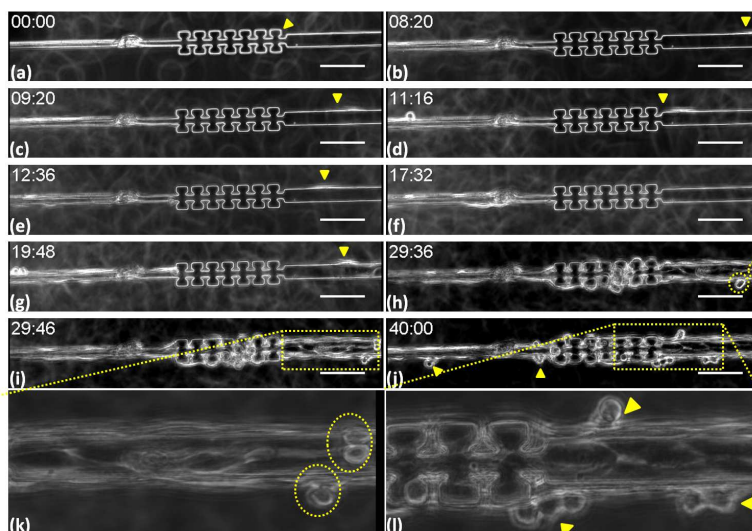


Fig. 3

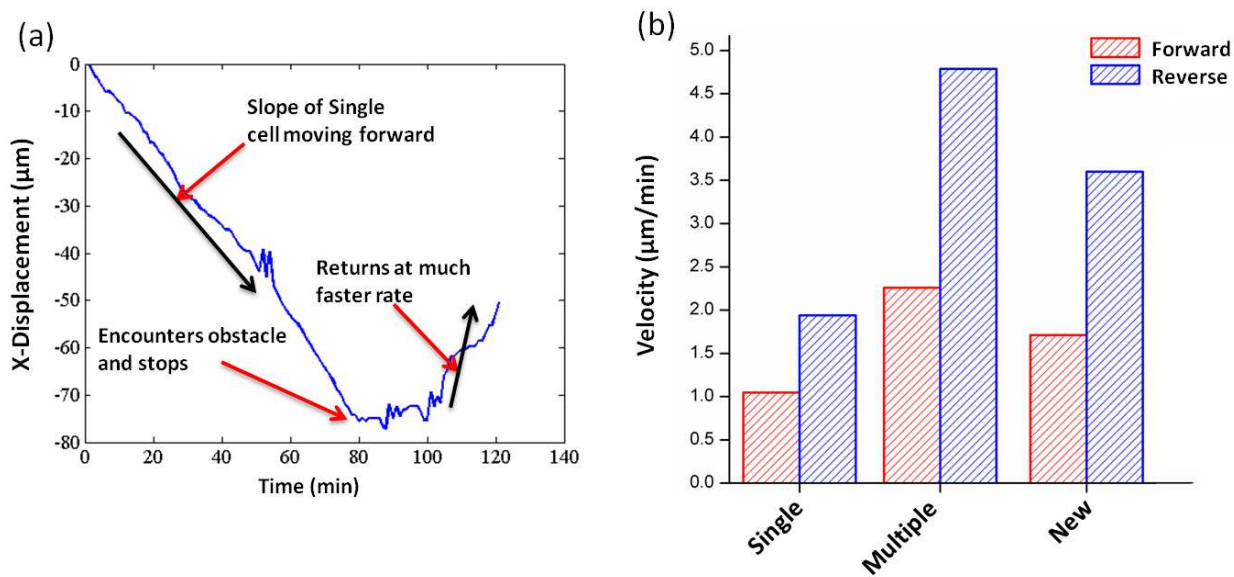


Fig. 4

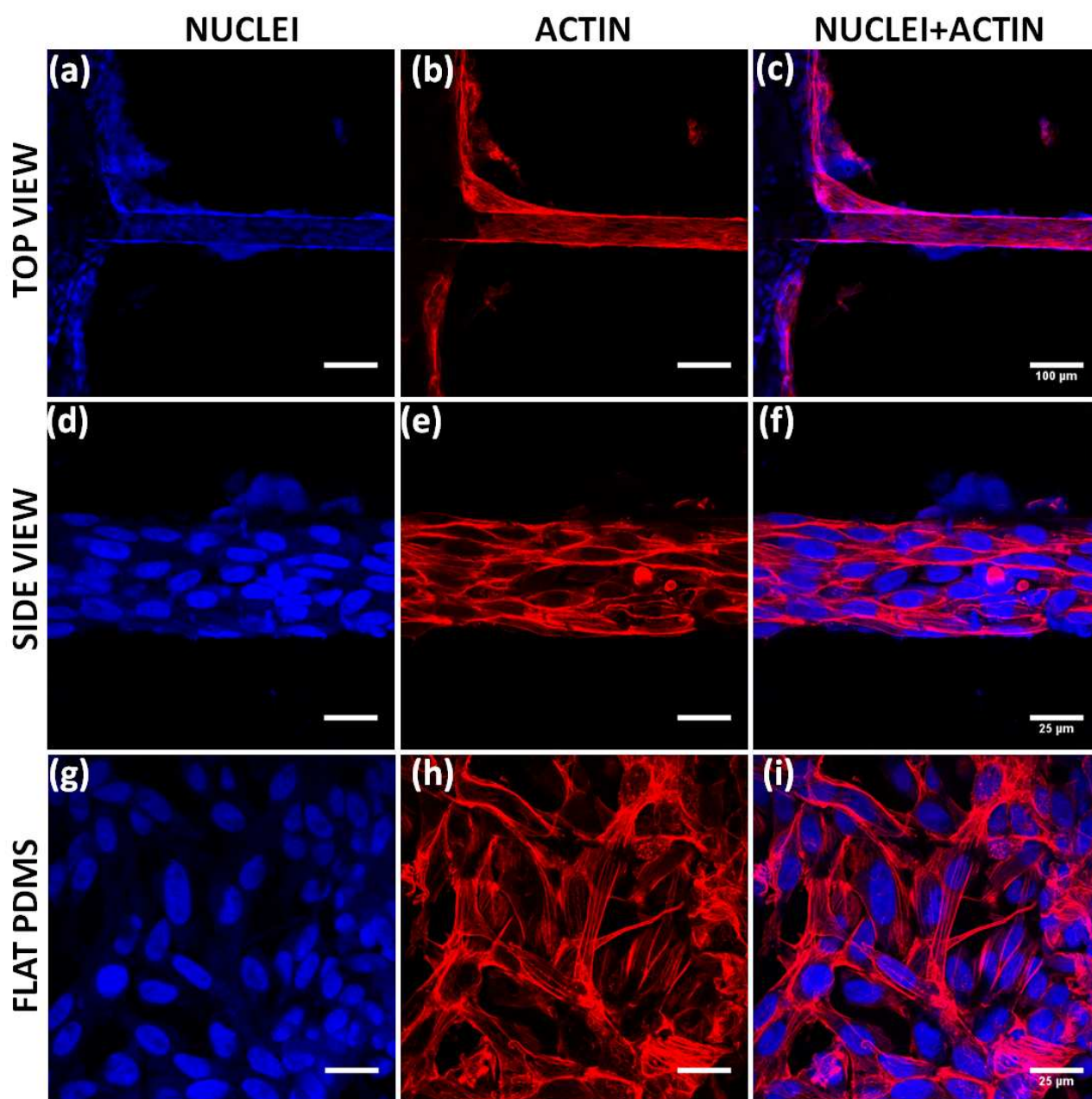


Fig. 5

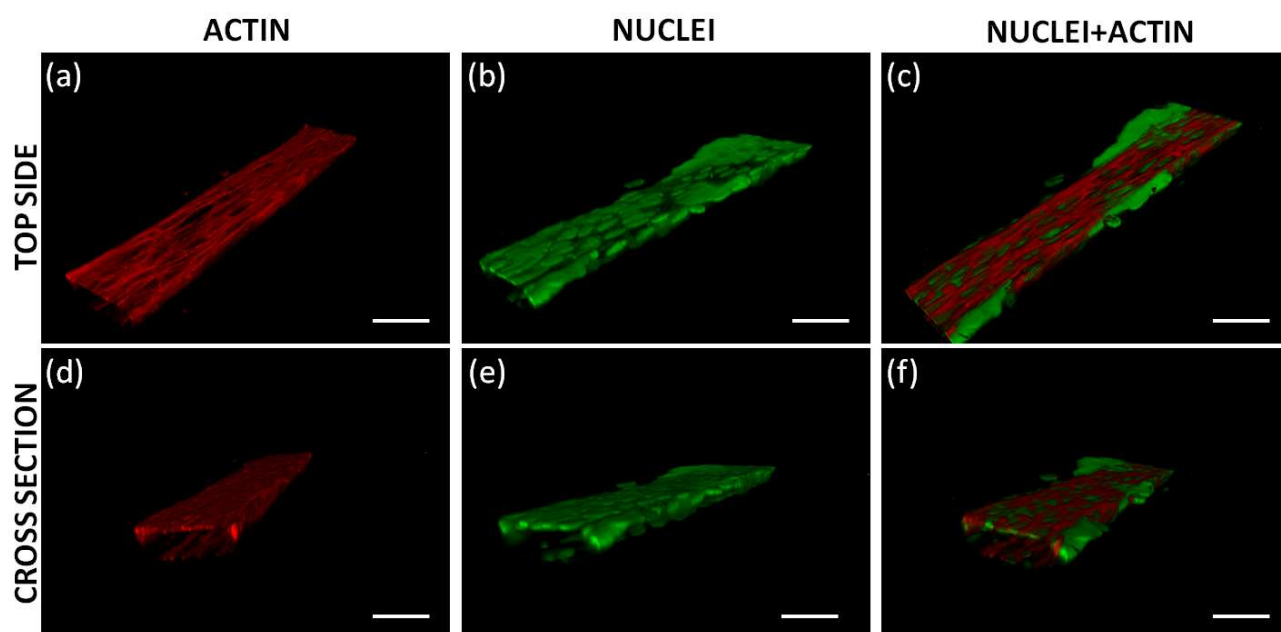


Fig. 6

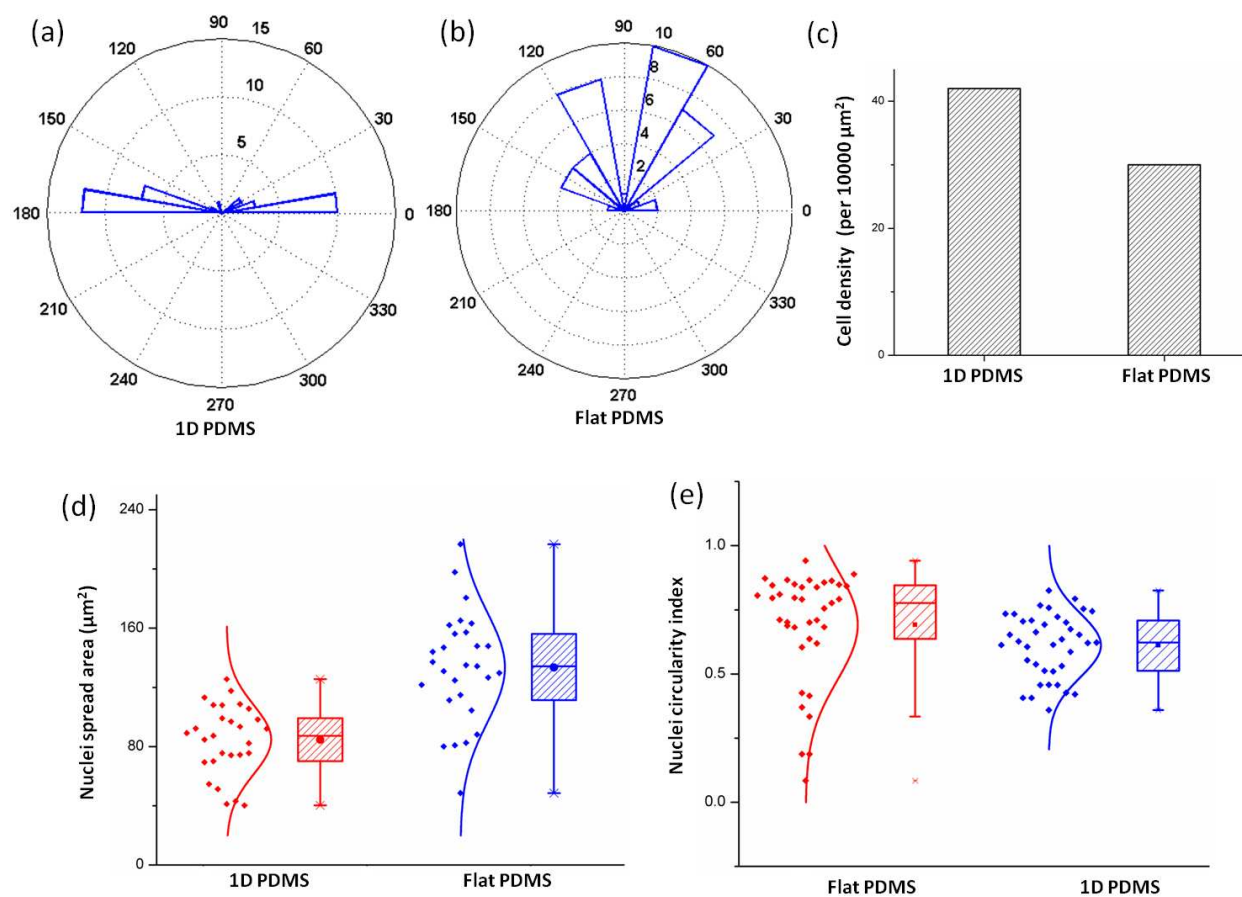
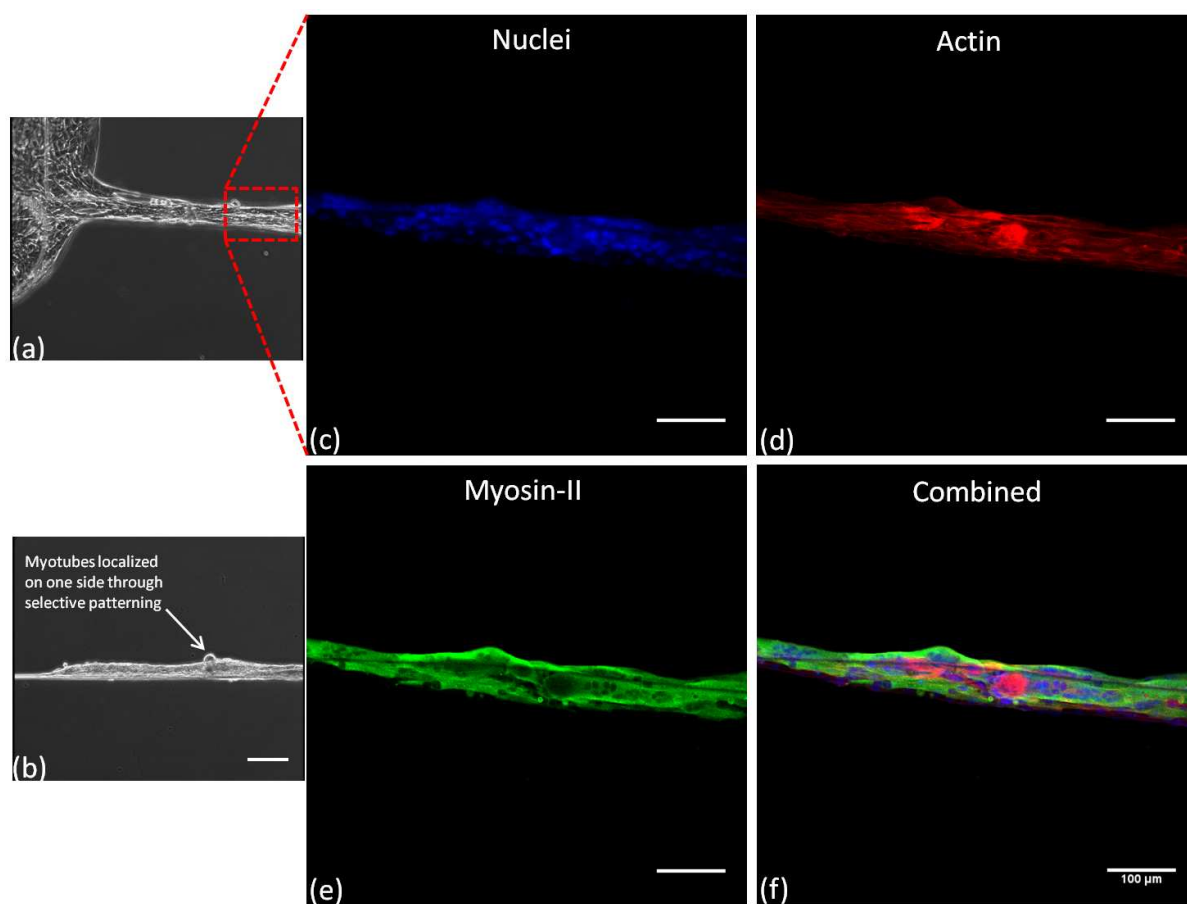


Fig. 7

**Fig. 8**

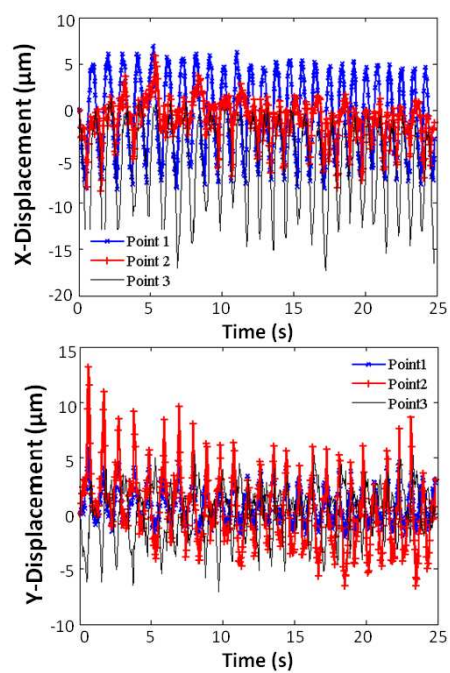
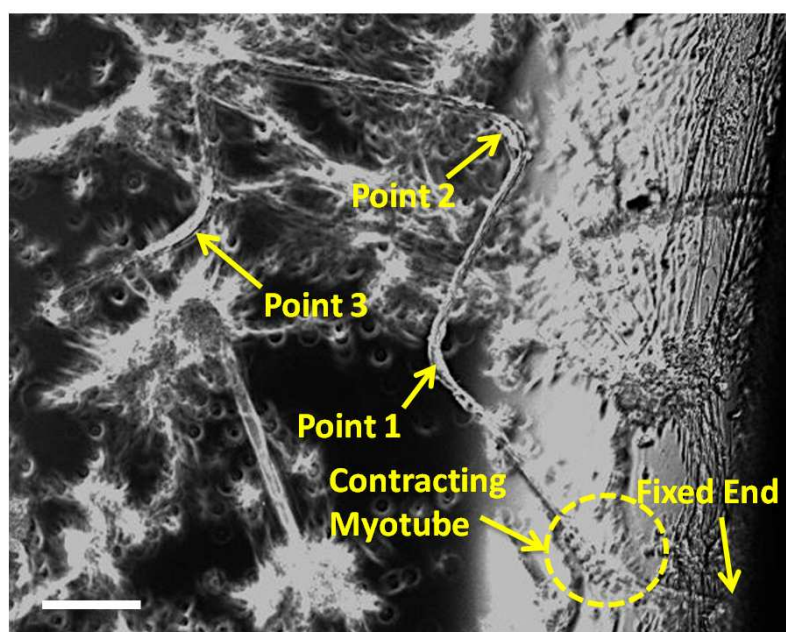


Fig. 9